AD-A280 936

REPORT DO:

1a. REPORT SECURITY CLASSIFICATION Unclassified	
2a. SECURITY CLASSIFICATION AUTHORITY	**3. DISTRIBUTION / AVAILABILITY OF REPORT** This document has been approved for public
2b. DECLASSIFICATION / DOWNGRADING SCHEDULE	release and sale; it's distribution is unlimited
4. PERFORMING ORGANIZATION REPORT NUMBER(S) Technical Report #3	**5. MONITORING ORGANIZATION REPORT NUMBER(S)** 4133046

DTIC
ELECTE
S
JUL 01 1994
F
D

6a. NAME OF PERFORMING ORGANIZATION University of Minnesota	**6b. OFFICE SYMBOL** *(If applicable)* ONR	**7a. NAME OF MONITORING ORGANIZATION** Office of Naval Research
6c. ADDRESS (City, State, and ZIP Code) Dept. of Chemical Eng. & Materials Science University of Minnesota Minneapolis, MN 55455		**7b. ADDRESS (City, State, and ZIP Code)** 800 Quincy Street North Arlington, VA 22217-5000
8a. NAME OF FUNDING / SPONSORING ORGANIZATION Office of Naval Research	**8b. OFFICE SYMBOL** *(If applicable)* ONR	**9. PROCUREMENT INSTRUMENT IDENTIFICATION NUMBER** Grant N00014-93-1-0563

8c. ADDRESS (City, State, and ZIP Code)	**10 SOURCE OF FUNDING NUMBERS**			
800 North Quincy Street Arlington, VA 22217-5000	PROGRAM ELEMENT NO.	PROJECT NO.	TASK NO.	WORK UNIT ACCESSION NO

11. TITLE (Include Security Classification)

Self-Assembly of Low-Dimensional Conductors on Au(111) Surfaces

12. PERSONAL AUTHOR(S)
J. Hossick Schott and M. D. Ward

13a. TYPE OF REPORT Technical	**13b. TIME COVERED** FROM 5/1/93 TO 6/30/94	**14. DATE OF REPORT (Year, Month, Day)** 6/23/94	**15. PAGE COUNT** 30

16. SUPPLEMENTARY NOTATION

17.	**COSATI CODES**		**18. SUBJECT TERMS** *(Continue on reverse if necessary and identify by block number)*
FIELD	**GROUP**	**SUB-GROUP**	Organic Conductors/Atomic Force Microscopy/Nucleation/
			Fractals

19. ABSTRACT *(Continue on reverse if necessary and identify by block number)*

Two-dimensional nanoclusters of (TTF)(TCNQ) (TTF = tetrathiafulvalene, TCNQ = tetracyano-quinodmethane) and Li^+TCNQ^-, formed on Au(111) surfaces by vapor phase sublimation under ambient conditions prior to growth of bulk crystals of these low-dimensional organic conductors, have been observed with scanning tunneling microscopy (STM) and scanning electron microscopy (SEM). The molecular planes of the constituents in individual nanoclusters are oriented perpendicular to the Au(111) substrate, while the clusters exhibit azimuthal orientations conforming to the threefold Au <110> directions. The nanocluster morphology and structure suggest that self-assembly of the nanoclusters is governed by specific interactions between the molecular species and the substrate and molecular diffusion along <110> troughs on the Au(111) substrate surface. In the case of the (TTF)(TCNQ) nanoclusters, TTF and TCNQ molecules assemble into molecular rows normal to the stacking direction, with intermolecular distances along the stacking direction which are nearly identical to those observed in bulk (TTF)(TCNQ). In contrast, the intermolecular spacings between TCNQ molecules along the

20. DISTRIBUTION / AVAILABILITY OF ABSTRACT ☒ UNCLASSIFIED/UNLIMITED ☐ SAME AS RPT ☐ DTIC USERS	**21. ABSTRACT SECURITY CLASSIFICATION** Unclassified	
22a. NAME OF RESPONSIBLE INDIVIDUAL Robert Nowak	**22b. TELEPHONE (Include Area Code)** (612) 703-696-4409	**22c. OFFICE SYMBOL** ONR Code 1113

DD FORM 1473, 84 MAR 83 APR edition may be used until exhausted. SECURITY CLASSIFICATION OF THIS PAGE
All other editions are obsolete.

Unclassified

molecular stacking axis in Li^+TCNQ^- nanoclusters are substantially larger than that observed in bulk M^+TCNQ^- salts. The large intermolecular spacing in Li^+TCNQ^- nanoclusters is consistent with Coulomb repulsion between fully reduced $\rho = 1$ $TCNQ^-$ anion sites in the Li^+TCNQ^- nanoclusters (ρ = formal charge). The smaller spacings observed for (TTF)(TCNQ) nanoclusters is consistent with reduced Coulomb repulsion, in agreement with the fractional charge known to exist in the bulk material ($\rho = 0.59$ and 0.59^- for TTF and TCNQ sites, respectively). The preferred direction of growth of the nanoclusters is <u>transverse</u> to the molecular stacking axes in both compounds, whereas the macroscopic morphologies reflect preferred growth <u>parallel</u> to the stacking direction. These observations indicate that morphology and molecular packing of crystal nuclei at the nanoscale are not necessarily identical to the corresponding characteristics observed at the macroscopic scale.

OFFICE OF NAVAL RESEARCH

GRANT # N00014-93-1-0563

R&T Code 4133046

Technical Report # 3

"Self-Assembly of Low-Dimensional Conductors on Au(111) Surfaces"

by

J. Hossick Schott and M. D. Ward

Prepared for Publication

in the

Journal of the American Chemical Society

Department of Chemical Engineering and Materials Science
University of Minnesota
Amundson Hall
421 Washington Ave. SE
Minneapolis, MN 55455

June 20, 1994

94-20226

94 7 1 027

Self-Assembly of Low-Dimensional Molecular Nanoclusters
on Au(111) Surfaces

Joachim Hossick Schott and Michael D. Ward*

Department of Chemical Engineering and Materials Science,

University of Minnesota, 421 Washington Ave. SE, Minneapolis 55455

Abstract

Two-dimensional nanoclusters of (TTF)(TCNQ) (TTF = tetrathiafulvalene, TCNQ = tetracyanoquinodmethane) and Li^+TCNQ^-, formed on Au(111) surfaces by vapor phase sublimation under ambient conditions prior to growth of bulk crystals of these low-dimensional organic conductors, have been observed with scanning tuneling microscopy (STM) and scanning electron microscopy (SEM). The molecular planes of the constituents in individual nanoclusters are oriented perpendicular to the Au(111) substrate, while the clusters exhibit azimuthal orientations conforming to the threefold Au <110> directions. The nanocluster morphology and structure suggest that self-assembly of the nanoclusters is governed by specific interactions between the molecular species and the substrate and molecular diffusion along <110> troughs on the Au(111) substrate surface. In the case of the (TTF)(TCNQ) nanoclusters, TTF and TCNQ molecules assemble into molecular rows normal to the stacking direction, with intermolecular distances along the stacking direction which are nearly identical to those observed in bulk (TTF)(TCNQ). In contrast, the intermolecular spacings between TCNQ molecules along the molecular stacking axis in Li^+TCNQ^- nanoclusters are substantially larger than that observed in bulk M^+TCNQ^- salts. The large intermolecular spacing in Li^+TCNQ^- nanoclusters is consistent with Coulomb repulsion between fully reduced $\rho = 1$ $TCNQ^-$ anion sites in the Li^+TCNQ^- nanoclusters (ρ = formal charge). The smaller spacings observed for (TTF)(TCNQ) nanoclusters is consistent with reduced Coulomb repulsion, in agreement with the fractional

charge known to exist in the bulk material ($\rho = 0.59^+$ and 0.59^- for TTF and TCNQ sites, respectively). The preferred direction of growth of the nanoclusters is *transverse* to the molecular stacking axes in both compounds, whereas the macroscopic morphologies reflect preferred growth *parallel* to the stacking direction. These observations indicate that morphology and molecular packing of crystal nuclei at the nanoscale are not necessarily identical to the corresponding characteristics observed at the macroscopic scale.

---

*Author to whom correspondence should be addressed

Version 1.4   06.19.94

To be submitted to *Langmuir*

Accesion For	
NTIS CRA&I	☑
DTIC TAB	☐
Unannounced	☐
Justification	
By	
Distribution /	
Availability Codes	
Dist	Avail and / or Special
A-1	

Introduction

The self-assembly of molecular species into ordered arrays is crucial to several areas of fundamental and technological interest. Liquid crystals exhibit rich phase behavior due to molecular ordering on mesoscopic length scales.[1] The properties of photographic dyes and sensitizers are influenced significantly by aggregate structure and molecular orientation with respect to a substrate. Molecular self-assembly also plays an important role in the nucleation of growth of molecular crystals, and is a key determinant of crystal characteristics such as polymorphism and morphology. While crystal engineering strategies for the design and synthesis of molecular crystals have been explored extensively,[2] the self-assembly and molecular recognition principles responsible for nucleation and growth have begun to emerge only recently. Several recent examples of molecular self-assembly have revealed the importance of substrate interfaces during heterogeneous nucleation. Molecular recognition between prenucleation aggregates and well-defined interfaces such as Langmuir monolayers,[3] self-assembled monolayers,[4,5] and single crystal substrates[6] has been shown to influence growth orientation, nucleation rates, and polymorphism of molecular crystals.

Molecular-based electronic devices, which may provide unprecedented control of structure and properties, will be realized only when the self-assembly of the molecular constituents leading to these materials can be directed in a preordained manner. Epitaxially driven formation of ordered molecular assemblies of organic molecules such as coronene and phthalocyanines on van der Waals solid substrate surfaces has been reported recently, suggesting routes to the fabrication of molecular heterojunctions.[7] In this regard, we have been interested in the formation of molecular assemblies on solid substrates in which the assemblies derive from redox active species commonly found in low-dimensional conducting solids. The formation of these assemblies on metal substrate surfaces is particularly interesting because low-dimensional conductors are commonly synthesized by electrochemical crystallization on metal electrodes. Little is known about the early stages of the electrochemical nucleation and growth of these compounds, although recent atomic force microscopy investigations have provided insight into

3

crystallization in the nanoscopic regime.[8]   We have demonstrated recently the formation, by vapor phase sublimation, of ordered nanoclusters of (TTF)(TCNQ), a low-dimensional metal in the bulk, on Au(111) surfaces.[9] Scanning tunneling microscopy (STM) studies revealed the formation of two types of clusters. The predominant clusters (Type I) were monolayer and multilayer (TTF)(TCNQ) assemblies resembling the *ac* face of bulk (TTF)(TCNQ), with the molecular planes parallel to the Au(111) surface. This orientation was preserved as the clusters grew into macroscopic crystals.   These studies also revealed, however, a minor amount of clusters assigned as Type II, in which the molecular planes were normal to the Au(111) surface. If the cluster assumes a molecular motif resembling the bulk phase, this orientation dictates that one-dimensional stacks of TTF and TCNQ molecules are parallel to the Au(111) surface.
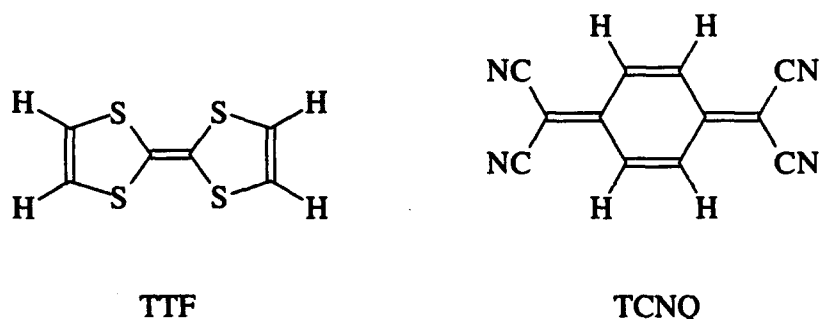
TTF   TCNQ

We describe herein the structure and properties of Type II nanoclusters of (TTF)(TCNQ), as well as nanoclusters of the semiconducting charge-transfer salt Li^+TCNQ^- molecules.   In contrast to (TTF)(TCNQ), the latter forms only Type II clusters.   The molecular motifs of these clusters resemble those of the bulk crystals, although intermolecular Coulomb repulsions and strong substrate-adsorbate interactions are suggested by uncharacteristically large interplanar spacings along the stacking direction.   In both systems, the preferred growth direction of the adsorbed crystal nuclei is dictated by the symmetry and structure of the substrate surface. Particularly revealing is the morphology of the nanoclusters in which their molecular stacking axes are parallel to the short axis of the cluster, opposite to that observed in macroscopic crystals of these materials grown on identical surfaces.   The characteristics of these clusters reveals the

4

interplay between substrate structure, molecular surface diffusion, adsorbate-substrate interactions on metal surfaces, and the important role of the substrate in the early stages of nucleation and growth.

Experimental Section

Substrate preparation. Au(111) surfaces were prepared according to a previously described procedure.[10,11,12] One end of a ~2 cm piece of Au-wire (99.999 % purity, 0.5 mm diameter, Johnson Matthey) was melted in a hydrogen-oxygen flame to form a sphere of 1 - 2 mm diameter. Upon cooling in air, highly reflective facets appeared on the sphere which proved to be atomically flat in STM. High resolution STM exhibited the unreconstructed phase of the Au(111) surface.

Sample preparation. Nanoclusters of (TTF)(TCNQ) or Li^+TCNQ^- were prepared on fresh Au(111) surfaces by positioning the Au substrate ~5 mm above (TTF)(TCNQ) or Li^+TCNQ^- crystals contained in a small vial at ambient pressure and temperature. Under these conditions, the vapor pressure of the charge-transfer salts was sufficient to obtain monolayer-thick nanoclusters within approximately five minutes, with longer times leading to thicker clusters. Crystals of meso- and macroscopic dimensions (0.1 - 100 μm^3) were prepared by sublimation at slightly higher temperatures (60° C) and longer times (up to ~15 hours). STM images were acquired in ambient air using a Nanoscope II$^{(TM)}$ scanning tunneling microscope equipped with a mechanically cut Pt(90%)Ir(10%) tip, with the tip held at virtual ground. Images were acquired in the constant current mode. Based on atomically resolved images of Au(111) surfaces, the lateral accuracy of the STM data is estimated as ± 0.3Å. All images consist of 400 x 400 data points and were obtained with a scan rate of 8.6 Hz.

Results and Discussion

Nanocluster morphology. Brief exposure of a flame annealed gold sphere, containing atomically flat Au(111) facets, to (TTF)(TCNQ) or Li$^+$TCNQ$^-$ vapor under ambient conditions resulted in the formation of nanometer-scale clusters on the Au substrate that could be observed readily by STM (Figure 1, 2). The tunneling conditions significantly influenced the ability to observe the nanoclusters, as low set-point resistances often resulted in the destruction of the clusters. Therefore, all images were obtained using set-point resistances $\geq$ 1 GΩ. Sublimation of either TTF or TCNQ alone afforded only disordered, poorly defined crystals on the surface.

[Figure 1]

[Figure 2]

The STM data in Figure 1 actually reveal that two different types of (TTF)(TCNQ) nanoclusters can be distinguished. Large, irregularly shaped "Type I" nanoclusters having a sheet-like morphology (Figure 1A) and an apparent height of 1.3 Å (as measured with respect to the underlying Au(111) surface) predominate, whereas "Type II" nanoclusters exhibiting worm-like morphologies and apparent heights of 1.6 Å are observed only infrequently (Figure 1B). The Type I nanoclusters, which we have described previously in detail,[7] exhibit random azimuthal orientation with the TTF and TCNQ molecular planes parallel to the Au(111) surface. However, the Type II nanoclusters are highly oriented, the long axes of different clusters subtending angles of 60° or 120°. In Figure 1B these nanoclusters are predominantly oriented parallel to the edges of large defects on the Au(111) surface which have a depth of one atomic layer. The edges of these defects most likely comprise steps oriented along the <110> directions of the Au(111) substrate since the step edges subtend angles of 60° and 120°. This observation indicates that self-assembly of the Type II nanoclusters preferentially occurs along directions conforming to the threefold symmetry of the Au(111) surface, specifically along the <110> directions which define atomic "troughs" on the (111) plane.

Nanoclusters of Li$^+$TCNQ$^-$ are also evident after exposure of the Au(111) substrate to this charge-transfer salt. In this case the Type I morphology has never been observed. Rather, only worm-like nanoclusters, resembling the Type II (TTF)(TCNQ) nanoclusters, are observed. The apparent height of these clusters also is 1.6 Å, and the long axes of different clusters form angles of 60° and 120° with respect to each other. Apparently, self-assembly of the Li$^+$TCNQ$^-$ nanoclusters also conforms to the threefold symmetry of the Au(111) surface.

Molecular architecture. Higher resolution STM images of the Type II (TTF)(TCNQ) clusters reveal parallel rows of contrast with center-to-center spacings between rows ranging from a minimum of 3.6 Å to a maximum of 4.9 Å (Figure 3). These rows are always parallel to the long axis of the nanoclusters. Each row consists of repeating tunneling current maxima, with distances between maxima ranging from 2.8 to 4.0 Å (Figure 3B). This pattern is consistent with the structural motif expected for a (TTF)(TCNQ) monolayer in which the molecular motif resembles that of the (10$\bar{1}$) plane of the bulk crystal, with TTF and TCNQ molecules alternating along the row direction but forming segregated stacks transverse to the rows (Figure 3C).[13] Consideration of the TTF HOMO and TCNQ LUMO (Figure 3D), which describe the states nearest the Fermi level in the bulk material based on a tight-binding approximation,[14] suggests that the tunneling current observed on this plane would exhibit two maxima per TTF molecule (corresponding to the sulfur atoms) and three maxima per TCNQ molecule (corresponding approximately to the two methylidene carbons and the ring orbitals). A computer generated overlay of the TTF HOMO and TCNQ LUMO states based on the (10$\bar{1}$) plane of crystalline (TTF)(TCNQ) is in reasonable agreement with the STM data (crystal structure lattice parameters: b = 3.819 Å, [101] = 21.48 Å; STM data: b = 4.4 Å (average spacings between rows, measured along the b direction), [101] = 17 Å). While this model ignores the influence of the substrate on the wavefunctions and tunneling probability,[15] the STM data suggest the presence of segregated molecular stacks of TTF and TCNQ molecules (labelled a and b, respectively, in Figure 3A).

Based on the above assignment of molecular orientation, the observed nanocluster morphology indicates that the direction of fastest growth for the Type II (TTF)(TCNQ) nanoclusters is transverse to the stacking axis. This morphology contrasts with that observed for bulk crystals, which crystallize as needles with the needle axis coincident with the b stacking axis, signifying fast growth along the b direction. The substrate is clearly playing an important role in the mechanism of molecular self-assembly at small length scales where molecule-substrate interactions are important.

High resolution STM images of the Li^+TCNQ^- nanoclusters exhibit features resembling those of the Type II (TTF)(TCNQ) clusters (Figure 4). Parallel rows of tunneling current are observed which are aligned with the long axis of the cluster, with periodic tunneling current maxima within the rows. However, the spacing between the rows is more uniform and clearly larger, 4.6 - 4.9 Å, than that observed for the (TTF)(TCNQ) clusters. These spacings also are considerably larger than those observed in bulk alkali-TCNQ crystals ($\approx$ 3.8 Å). To our knowledge, no detailed x-ray structural analysis has been performed for Li^+TCNQ^-. Our attempts to grow single crystals of Li^+TCNQ^- were not successful as the crystals were either too small or were twinned. However, it is well established that the structure of other alkali TCNQ compounds such as Rb^+TCNQ^- and K^+TCNQ^- are isomorphous.[16] These salts crystallize in the $P2_1/c$ space group, with the structural data for K^+TCNQ^- reported as: a = 7.08 Å, b = 17.78 Å, c = 17.86 Å, β = 94.95°.[17,18,19] Notably, the angle subtended between rod-shaped vacancies of monomolecular width (one of these is labelled "V" in Figure 4B) and the row direction is 95°. This angle is identical to β for bulk K^+TCNQ^-, which is the angle subtending the stacking direction and the b axis, which is coincident with molecular rows of $TCNQ^-$ anions. This observation supports a nanocluster motif in which $TCNQ^-$ anions form one-dimensional molecular stacks transverse to molecular rows of $TCNQ^-$ anions, similar to the motif in bulk K^+TCNQ^-.

Close examination of the periodicity of tunneling current within the rows of a nanocluster reveals regions containing trimers and regions containing dimers *and* trimers of tunneling current

8

maxima (Figure 5 and Figure 6). The end-to-end distance for each trimer is $\approx$ 8 Å and $\approx$ 4 Å for each dimer, nearly identical to the distance between the nitrogen atoms along the long (8.2 Å) and the short axis (4.2 Å) of the TCNQ molecule, respectively. The observed tunneling features are consistent with TCNQ⁻ anions arranged end-to-end along the long molecular axis and/or in an up-sideways manner (Scheme 1), the latter resembling the motif in crystalline K⁺TCNQ⁻. Both arrangements are observed within a single cluster, however, the tunneling current contrast indicates that within a given stack the molecular orientations are identical. *Notably, the apparent stacking axis forms an angle of 95° with the direction of the dimer-trimer or trimer-trimer rows.* This, together with the fact that the stacks are composed of molecules adsorbed in one particular molecular orientation, strongly indicates that some bulk features of Li⁺TCNQ⁻ crystals are present even during the initial stages of nucleation. This suggests that intermolecular forces responsible for the bulk structure are operative in the monolayer, despite the fact that the intermolecular separation along the stacking axis in the nanoclusters is considerably larger than in bulk crystals. The Li⁺ ions, which presumably reside in the regions between the TCNQ stacks, are not expected to participate in tunneling due to their lack of states near the Fermi level. Furthermore, if the nanocluster mimicks the solid state structure, the Li⁺ ion is embedded in the nitrogen terminated arms of the TCNQ molecules, which would mitigate resolution of its tunneling features from those of TCNQ⁻. We exclude the possiblility that Li⁺TCNQ⁻ dissociates on the Au(111) surface to give stacks of neutral TCNQ molecules because STM of Au(111) substrates exposed to TCNQ alone did not yield comparable features.

Scheme 1

[Figure 4]

[Figure 5]

[Figure 6]

9

Intermolecular and substrate interactions in nanocluster self-assembly. As with the Type II (TTF)(TCNQ) clusters, the morphology of the Li^+TCNQ^- nanoclusters differs from that typically observed for macroscopic crystals of low-dimensional solids. That is, the preferred growth direction of the nanoclusters is approximately perpendicular to the $TCNQ^-$ stacking axes. This behavior is strong evidence that the Au(111) substrate plays an important role in the self-assembly of the nanoclusters. The role of the substrate is particularly evident from the relative orientations of the nanoclusters in a given image, and by their orientation with respect to the directions of steps on the Au(111) surface, which are surmised to be <110> directions that also define atomic "troughs" between rows of Au atoms on a defect-free Au(111) surface (see Figure 7). The angles subtended by the molecular rows in different clusters are 0°, 60°, and 120°, conforming to the three-fold symmetry of the <110> troughs (Figure 2, 4).

These results indicate that self-assembly along the <110> troughs is favorable, reflecting an interplay between intermolecular interactions, adsorbate-substrate interactions, and facile surface diffusion of molecular species in the <110> troughs. Self-assembly of diffusing molecules on the Au(111) surface can occur by two modes: (1) end-to-end alignment of molecular species in the <110> troughs, resulting in formation of oriented molecular chains and rapid cluster growth parallel to <110> of the Au substrate or (2) face-to-face stacking of TTF or TCNQ molecules across neighboring atomic troughs oriented roughly along the <221> direction. The morphology of the nanoclusters suggests that the flux of (TTF)(TCNQ) and Li^+TCNQ^- species along the <110> troughs is greater than along other directions, including <221>. This is reasonable for molecules whose planes are oriented perpendicular to the surface. If the molecules were to diffuse with their molecular plane parallel to the surface, in the absence of strong epitaxy no preferred growth direction of the clusters would be expected since the molecule would be too wide to fit in the atomic trough. Indeed, Type I (TTF)(TCNQ) clusters do not exhibit any azimuthal orientation whatsoever (Fig. 1A). Since Type II clusters are rarely observed in the case of (TTF)(TCNQ) but are observed exclusively for Li^+TCNQ^-, this implies that TTF and TCNQ molecules in (TTF)(TCNQ) adsorb predominantly with their molecular

10

planes aligned parallel to the Au(111) surface and Li$^+$TCNQ$^-$ molecules with their planes perpendicular to the surface. Epitaxially driven growth of the Type II clusters of either (TTF)(TCNQ) or Li$^+$TCNQ$^-$ by lattice matching of the Au(111) substrate and the crystallographic planes of the organic crystals is not likely as no reasonable lattice match with three-fold symmetry could be found. This observation therefore supports a self-assembly process which is governed by favorable adsorption of the TCNQ$^-$ anion and rapid diffusion in the <110> troughs. Notably, the distance between two nitrogen atoms along the long molecular axis is 8.2 Å, which is close to the 8.6 Å spacing between two threefold hollow sites along the direction of the atomic troughs (Figure 8). This agreement may provide for favorable binding of TCNQ$^-$ with the Au(111) substrate in the <110> troughs, thereby increasing the concentration of TCNQ$^-$ anions, and promoting their subsequent assembly, in the <110> troughs. This argument suggests that the predominance of Type I clusters for (TTF)(TCNQ) is due to a stronger preference of TTF to lay flat on the Au(111), possibly due to favorable gold-sulfur interactions.

[Figure 7]

[Figure 8]

The role of the <110> troughs is particularly evident in the STM images of the Li$^+$TCNQ$^-$ nanoclusters. The upper value measured for the spacing between molecular rows was 4.9 Å, nearly identical to the value of 5.0 Å traversed by two atomic rows along the <221> directions. This is good evidence that the TCNQ$^-$ anions reside in the troughs, which results in interplanar separations that are substantially larger than those observed in the solid state (3.34 Å and 3.74 Å for the intradimer and interdimer separations, respectively, in K$^+$TCNQ$^-$). Thus, diffusion and self-assembly of molecules along the atomic troughs of the Au(111) surface explains the worm-like morphology of both (TTF)(TCNQ) and Li$^+$TCNQ$^-$ nanoclusters, and their conformism to the three-fold symmetry of the Au(111) surface. Face-to-face stacking of molecules across neighboring atomic troughs is expected to instigate the formation of the

11

molecular stacking patterns present in (TTF)(TCNQ) and Li$^+$TCNQ$^-$ nanoclusters. In contrast to the interplanar spacings in Li$^+$TCNQ$^-$ clusters, the smallest measured separation between the parallel rows in the (TTF)(TCNQ) clusters was 3.9 Å, approaching the interplanar separations in the bulk crystal (3.55 Å). At these separations, the TTF and TCNQ molecules cannot be in registry with the <110> troughs along the <221> direction. A plausible explanation for these observations may stem from the difference in Coulomb repulsion in the two solids. It is well established that the excess charge on TTF and TCNQ sites is only $\rho = 0.59^+$ and $\rho = 0.59^-$, respectively.[20] In contrast, the charge on the TCNQ$^-$ anion sites in Li$^+$TCNQ$^-$ is $\rho = 1.0^-$, which leads to extensive Coulomb repulsion terms in the solid state, the formation of a Mott gap, and the observation of semiconducting behavior in the bulk material. It is feasible that Coulomb repulsion mitigates the charge-transfer driven assembly of TCNQ$^-$ anions in Li$^+$TCNQ$^-$ clusters. That is, the stabilization realized from charge-transfer may not be sufficient to overcome Coulomb repulsion and TCNQ$^-$-adsorbate interactions in the <110> troughs. Under these conditions, the intermolecular spacings in the Li$^+$TCNQ$^-$nanoclusters would be dictated by the 4.9 Å spacing between two <110> troughs.

In contrast, the lower limit of 3.9 Å for the spacings between rows in (TTF)(TCNQ) clusters is consistent with less significant Coulomb repulsion expected for this material, which would inhibit to a lesser degree the assembly of molecules by face-to-face charge-transfer interactions. However, that larger 4.9 Å spacings are also observed occasionally, suggesting a delicate balance between Coulomb repulsion, substrate-adsorbate interactions, and charge-transfer interactions. It is also possible that the regions exhibiting larger inter-row spacings may represent domains which are not completely assembled, as the larger spacings are generally observed near regions containing large vacancies. In this regard, the ordered motif is not observed in smaller clusters (not shown here), but is observed readily in larger clusters.

Evolution of a crystal. Prolonged exposure of the Au(111) surface to Li$^+$TCNQ$^-$ vapor results in the formation of needle shaped crystals on the surface with their long axes oriented parallel to

12

the substrate surface, as observed by scanning electron microscopy (Figure 9). The STM data strongly support a nanoclusters in which the stacking axes are parallel to the Au(111) substrate surface and nearly coincide with the *short* axis of the cluster. If these characteristics were preserved during growth of mature crystals from these clusters, the TCNQ stacking axis would remain parallel to the Au(111) substrate. However, the stacking axes would be parallel to the short axis of the crystals, contrary to the typical morphology of low-dimensional solids in which the crystal needle axis and the stacking axis coincide. This issue can be resolved by close inspection of the SEM micrographs of the crystals. The angle subtended by the needle axis and the edges at the ends of the crystals is $95°$, identical to β, the angle subtending the a stacking axis and the c axis of bulk K^+TCNQ^-. This clearly indicates that the preferred direction of growth of more mature crystals is *parallel* to the TCNQ stacking axis, in contrast to the growth behaviour of the nanoclusters.

[Figure 9]

The different morphologies of the nanoclusters and bulk crystals can be explained by the directing influence of the substrate on the characteristics of the monolayer thick nanoclusters. This influence will diminish at longer length scales where the crystal morphology of larger Li^+TCNQ^- growth centers will be governed by crystal surface energies and rates of attachment to the exposed crystal faces, resulting in morphologies similar to those typically observed for single crystals. However, azimuthal orientation of the mature crystals is clearly evident from SEM, which reveals that the crystal needle axes subtend angles of $0°$, $60°$, and $120°$ with respect to each other, identical to the mutual orientations observed for the nanoclusters. This observation indicates that the crystallographic orientation of the crystals with respect to the Au(111) substrate *remains fixed by the initial nanocluster orientation.* This requires that crystal growth from these precursor nuclei involve a transition to the bulk structure with retention of orientation. The transition for Type II clusters may involve reconstruction of the primary layer at the Au(111)

13

interface upon deposition of subseqent layers, growth of bulk material on the unreconstructed primary layer, or a gradual evolution of the crystal lattice toward the bulk structure as the growth interface moves further from the substrate, which would involve gradual contraction along the *a* axis. Retention of azimuthal orientation in the mature crystals is evidence that the interaction between the primary layer and subsequent layers must be epitaxial in nature.

Conclusion

These studies clearly reveal that interactions between a substrate and nuclei play an important role in determining several crystal characteristics such as morphology and orientation. In the examples described here, the substrate also governs the molecular motif of the nanoclusters, which differs from the bulk crystals with respect to the intermolecular distances. Nevertheless, the orientation and motif established in the nanoclusters dictate the growth process leading to macroscopic crystals, as azimuthal and normal orientation is preserved. We anticipate that characterization of the nucleation and growth of organic crystals at the nanoscale level on well-defined substrates such as Au(111), will provide the fundamental understanding required for better control of the crystallization of these materials and, possibly, fabrication of novel devices where morphology, orientation, and molecular structure are crucial.

14

References

[1](a) Collings, P. J., *Liquid Crystals*, Princeton University Press (Princeton), **1990**. (b) Luckhurst, G. R.; Gray, G. W., *The Molecular Physics of Liquid Crystals*, Academic Press (New York), **1979**.

[2] (a) Miller, J.S. ; Epstein, A.J.; Reiff, W.M. *Science* **1988**, *240*, 40. (b) Miller, J.S. *Extended Linear Chain Compounds* (Plenum, New York, 1982-3), Vol. 1-3. (c) Garito, A.F.; Heeger,A.J. *Acc. Chem. Res.* **1974**, 7, 232. (d) Torrance, J.B. *Acc. Chem. Res.* **1979**, *12*, 79. (e) Zyss, J.; Tsoucaris, G. *Structure and Properties of Molecular Crystals*, Pierrot, M., Ed. (Elsevier, Amsterdam, 1990), pp. 297-350.

(a) Schmidt, G. M. J. *Pure Appl. Chem.* **1971**, *27*, 647. (b) Desiraju, G. *Crystal Engineering - The Design of Organic Solids* (Elsevier, New York, 1989). (c) Lehn,J. M. *Angew. Chem., Int. Ed. Eng.* **1988**, *27*, 89. (d) Fagan, P.J. ; Ward, M.D.; Calabrese, J. C. *J. Am. Chem. Soc.* **1989**, *111*, 1698.

[3](a) Landau, E. M.; Grayer Wolf, S; Levanon, M.; Leiserowitz, L.; Lahav, M.; Sagiv, J. *J. Amer. Chem. Soc.* **1989**, *111*, 1436. (b) Landau, E. M.; Grayer Wolf, Sagiv, J.; Deutsch, M.; Kjaer, K.; Als-Nielsen, J.; Leiserowitz, L.; Lahav, M. *Pure and Appl. Chem.* **1989**, *61*, 673. (c) Weissbuch, I.; Frolow, F.; Addadi, L.; Lahav, M.; Leiserowitz, L. *J. Amer. Chem. Soc.* **1990**, *112*, 7718.

[4]Frostman, L. M.; Ward, M. D. *Langmuir* **1994**,*10*, 576.

[5]Carter, P. W.; Ward, M. D. *J. Amer. Chem. Soc.* **1994**, *116*, 769.

[6]Carter, P. W.; Ward, M. D. *J. Amer. Chem. Soc.* **1993**, *115*, 11521.

[7]Collins, G. E.; Nebesny, J. W.; England, C. D.; Chau, L. K.; Lee, P. A.; Parkinson, B. A.; Armstrong, N. R. J. *Vac. Sci. Technol. A*, **1992**, *10*, 2902.

[8](a) Carter, P. W.; Hillier, A. C.; Ward, M. D. *J. Amer. Chem. Soc.* **1994**, *116*, 944. (b) Hillier, A. C.; Ward, M. D. *Science*, **1994**, *268*, 1261.

[9] Hossick Schott, J. ; Ward, M.D. *J. Am. Chem. Soc.*, in press.

[10] Hossick Schott, J. ; White, H.S. *Langmuir* **1992**, *8*, 1955.

[11] Hossick Schott, J.; Arana, C. R.; Abruña, H. D.; Petach, H. H.; Elliott, C.M.; White, H.S. *J. Phys. Chem.* **1992**, *96*, 5223.

[12] Hsu, T.; Cowley, T.M. *Ultramicroscopy* **1983**, *11*, 125.

[13] Kistenmacher, T.J.; Philipps, T.E.; Cowan, D.O. *Acta Cryst.* **1973**, *B30*, 763. The lattice parameters for (TTF)(TCNQ) are: $a = 12.298$ Å, $b = 3.819$ Å, $c = 18.468$ Å, $\beta = 104.46°$.

[14] Lowe, J. P.; *J. Am. Chem. Soc.* **1980**, *102*, 1262.

[15] Lang, N.D. *Phys. Rev. B.* **1986**, *34*, 5947.

[16]This is further suggested by the fact that the electronic properties of the salts are also very similar[20] ($\sigma_{Li+TCNQ-} = 5 \times 10^{-6} \ \Omega^{-1}cm^{-1}$; $\sigma_{K+TCNQ-} = 2 \times 10^{-6} \ \Omega^{-1}cm^{-1}$). We do note, however, that powder X-ray patterns obtained from both $Li^{+}TCNQ^{-}$ and $K^{+}TCNQ^{-}$ differed somewhat. Some peaks in the diffraction pattern of $Li^{+}TCNQ^{-}$ were shifted to slightly higher 2θ values compared to $K^{+}TCNQ^{-}$, suggesting smaller d-spacings. However, additional peaks also were detected, suggesting the presence of a different polymorph.

[17] Richard, P.; Zanghi, J.-C.; Guedon, J.-F.; Hota, N. *Acta Cryst.* **1978**, *B34*, 788.

[18] Konno, M.; Ishii, T.; Saito, Y. *Acta Cryst.* **1977**, *B33*, 763.

[19] Hoekstra, A.; Spoelder, T.; Vos, A. *Acta Cryst.* **1972**, B28, 14

[20] Melby, L.R.; Harder, R.J., Hertler, W.R., Mahler, W., Benson, R.E.; Mochel, W.E. *J. Am.Chem. Soc.* **1962**, 84, 3374.

Figure Captions

Figure 1. (A) Type I (TTF)(TCNQ) nanocluster on Au(111). The apparent height of these clusters is 1.3 Å, suggesting a monolayer thickness with the molecular planes parallel to the Au(111) surface. High resolution images are consistent with the a molecular motif resembling the *ac* face of the bulk crystal (see reference 2 for details). (B) Type II (TTF)(TCNQ) clusters. The clusters are worm-shaped, the long axes of the clusters subtending angles of 0°, 60°, and 120°. The feature denoted as "A" is a Au(111) terrace recessed below the upper substrate terrace by a depth corresponding to a monoatomic thickness (1.44 Å). This feature exhibits step directions which subtend angles of 60°, 120°, 180°, and 240°. These step directions most likely belong to the <110> family, contained in {001} step planes. The (TTF)(TCNQ) clusters appear to be oriented parallel to the <110> step directions. All images are low pass filtered once. Tunneling conditions: (a) V_b = -175 mV, i_T = 0.1 nA; (b) V_b = -225 mV, i_T = 0.1 nA; (c) V_b = -225 mV, i_T = 0.1 nA.

Figure 2. (A), (B) Li$^+$TCNQ$^-$ nanoclusters formed on a large Au(111) terrace, and at an Au(111) monoatomic step. Note that different clusters are oriented 60° and 120° with respect to each other and appear to grow with their long axes either parallel or at an angle of 60° or 120° with respect to the monoatomic steps. All images low pass filtered once. Tunneling conditions: (a) V_b = -75 mV, i_T = 0.1 nA; (b) V_b = -155 mV, i_T = 0.1 nA.

Figure 3. (A) High resolution STM data of a (TTF)(TCNQ) type II nanocluster. Parallel rows of tunneling current are evident, with spacings between rows ranging from a minimum of 3.5 Å to a maximum of 4.9 Å (measured normal to the rows). The distances between the periodic tunneling current maxima range between 2.8 Å and 4.0 Å, corresponding to intramolecular tunneling current pathways associated with TTF HOMO and TCNQ LUMO states. (B) A profile of the tunneling current within one of these rows. Tunneling conditions: V_b = -225 mV, i_T = 0.1 nA. (C) Molecular motif of the (10$\bar{1}$) plane of crystalline (TTF)(TCNQ). (D) The

TCNQ LUMO and TTF HOMO.[16] A computer generated model of the HOMO and LUMO of TTF and TCNQ, respectively, drawn to scale as viewed on the *ab* plane, is overlaid on the STM data in (A). The data is consistent with the presence of segregated TCNQ and TTF stacks (labeled a and b, respectively). The two tunneling current maxima comprising the features assigned to TTF molecules are attributed to the HOMO contributions on the two sulfur atoms nearest the tip. Two of the three tunneling current maxima comprising the features assigned to TCNQ molecules are attributed to the two nitrogen atoms nearest the tip at the termini of the molecule, the third to the central ring of the molecule.

Figure 4. (A), (B) High resolution STM images of Li$^+$TCNQ$^-$ nanoclusters. In (a), two clusters are observed whose long axes are oriented 120° with respect to each other. Parallel rows of tunneling current oriented along the long axes of the clusters are evident, with spacing between the rows of ≈ 4.8 Å. The clusters in (B) illustrate the typical morphology. Note that the angle between the rod-shaped vacancy of monomolecular width in the lower right corner of the image (labelled "V") forms an angle of 95° with the direction of the rows. The data in (a) are unfiltered and the data in (b) were low pass filtered once. Tunneling conditions: (a) V_b = -320 mV, i_T = 0.1 nA; (b) V_b = -224 mV, i_T = 0.1 nA. (C) Crystal structure of the *ac* plane of K$^+$TCNQ$^-$, illustrating the molecular anion stacks along *a* and the molecular rows of anions along *c*.

Figure 5. (A), (B). STM images of Li$^+$TCNQ$^-$ nanocluster illustrating tunneling current contrast which can be attributed to molecular TCNQ stacks. The image in (B) is a section of the image in (A) obtained by reducing the scanned area during data acquisition. Tunneling conditions: V_b = -235 mV, i_T = 0.1 nA. (c,d) STM images of a Li$^+$TCNQ$^-$ nanocluster which exhibits the "sideways-up" molecular architecture (see text). The image in (D) is a section of the image in (C) obtained by reducing the scanned area during data acquisition. Tunneling conditions are identical to those in (A). The data in (A) and (C) are unfiltered. The data in (B) and (D) are band-pass filtered to remove low frequency noise.

Figure 6. (A) Profiles of the tunneling current within one of the rows of a Li^+TCNQ^- nanocluster depicted in Figure 6C (lower trace), and of one of the rows in the image shown in Figure 6D (upper trace) are depicted. (B) A simplified representation of the TCNQ LUMO states,[16] based on the "end-to-end" motif, overlaid on the section of the data from Figure 6B at the same scale. (C) A simplified representation of the TCNQ LUMO states, based on the "sideways-up" motif, overlaid on the section of the data from Figure 6D at the same scale.

Figure 7. Schematic representation of the Au(111) surface, indicating the crystallographically equivalent <110> atomic troughs, along which molecular self-assembly of the nanoclusters is favored.

Figure 8. Schematic representation of quasi-epitaxial adsorption of a TCNQ molecule on Au(111), oriented perpendicular to the substrate with the long axis of the TCNQ molecule oriented parallel to <110>. The distance between two threefold hollow sites along <110> (8.6 Å) is nearly identical to the distance spanned by the terminal nitrogen atoms of TCNQ along the long axis of the molecule (8.2 Å).

Figure 9. (A) Scanning electron micrograph of Li^+TCNQ^- crystals grown on a facetted area of the Au(111) substrate (note the μm scale of these images). The needle axes of different crystals subtend angles of 0°, 60°, and 120°. (B) Scanning electron micrograph of a Li^+TCNQ^- crystal on Au(111). The angle in the lower right corner of the needle shaped crystal is measured to be 95°, indicating that the stacking axis of more mature crystals on the mesoscopic scale is parallel to the needle axis.
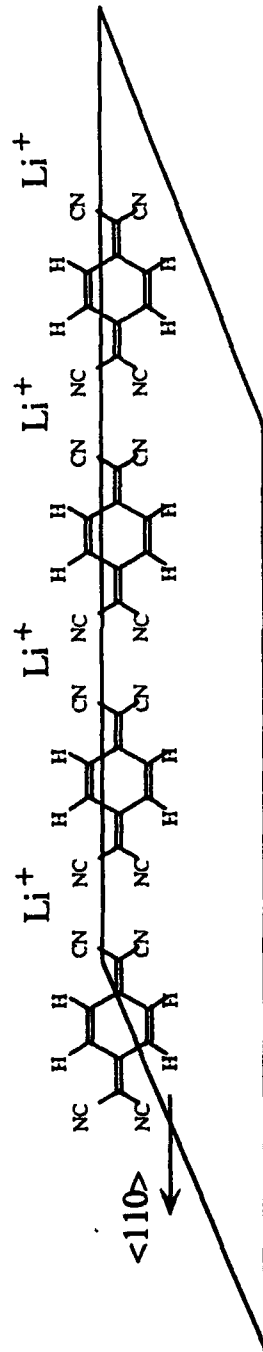
end-to-end
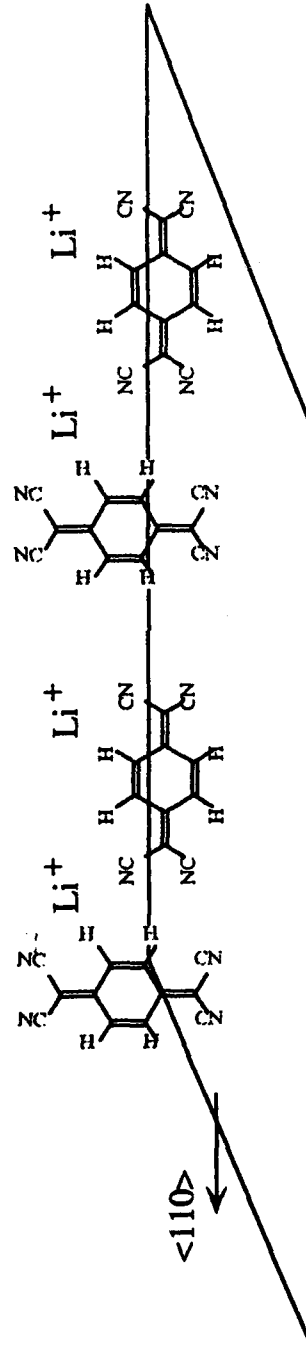
sideways-up

Scheme 1

A. 200 x 200 nm²

B. 250 x 250 nm²

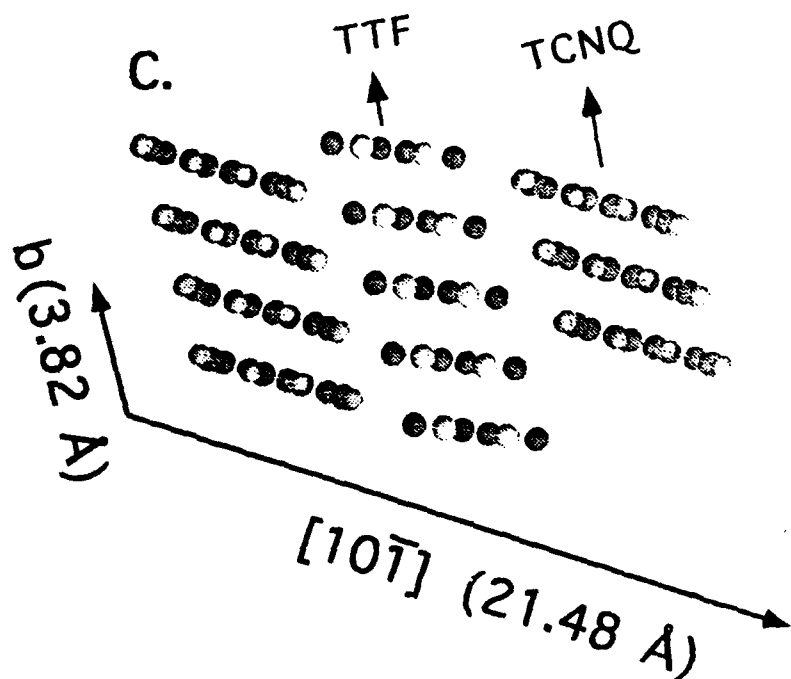Hossick Schott, Ward   Figure 1
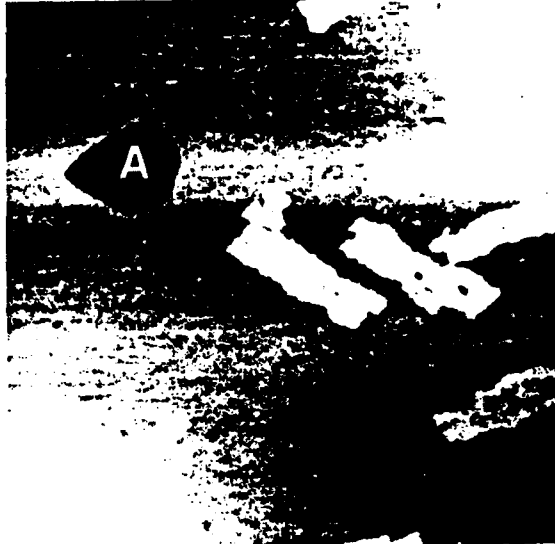
A. 250 x 250 nm²

B. 250 x 250 nm²
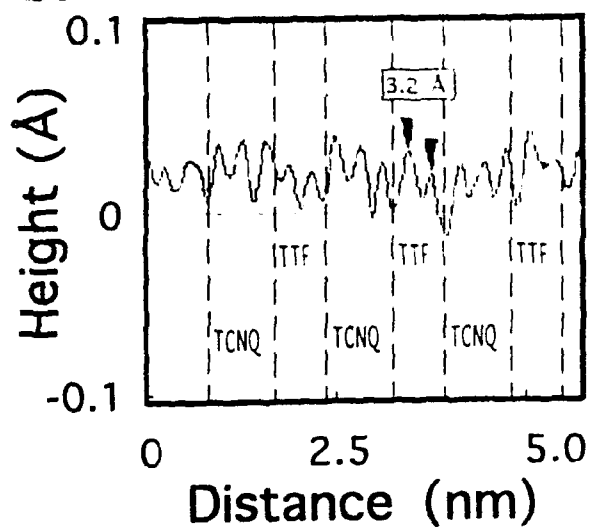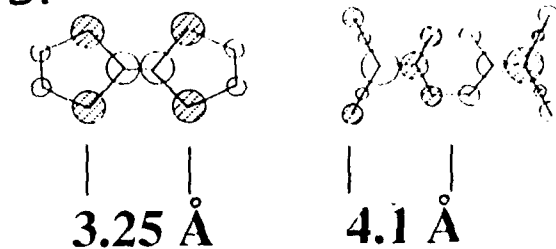
Hossick Schott, Ward   Figure 2

A. 5.5 x 5.5 nm^2

B.

C.

TTF   TCNQ

b(3.82 Å)

[10$\bar{1}$] (21.48 Å)

D.

3.25 Å   4.1 Å

Hossick Schott, Ward Figure 3

A. 18 x 18 nm²

B. 20 x 20 nm²

C.

Hossick Schott, Ward   Figure 4

A. 27.5 x 27.5 nm^2

B. 4.5 x 4.5 nm^2

C. 15 x 15 nm^2

D. 5 x 5 nm^2

Hossick Schott. Ward   Figure 5

A.
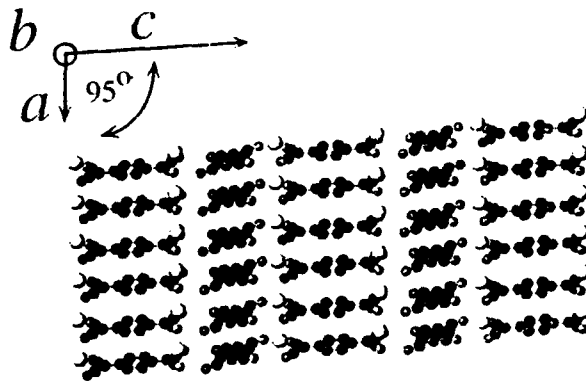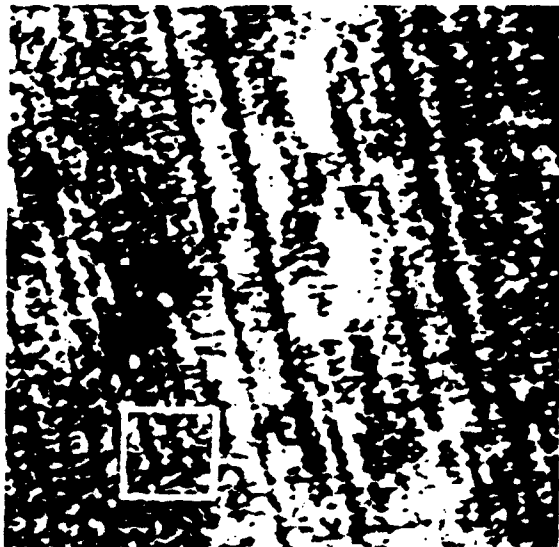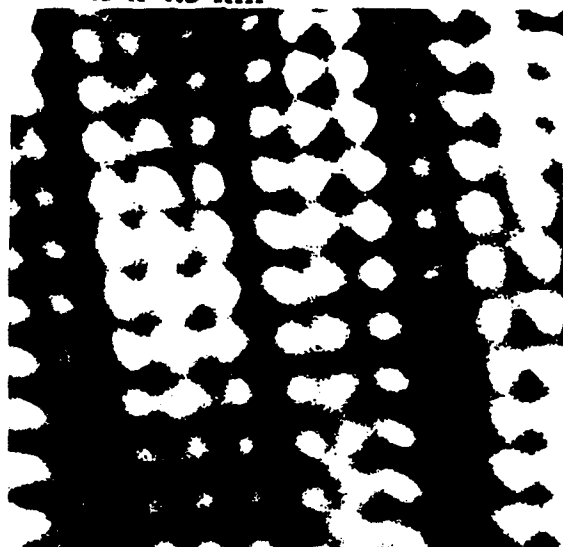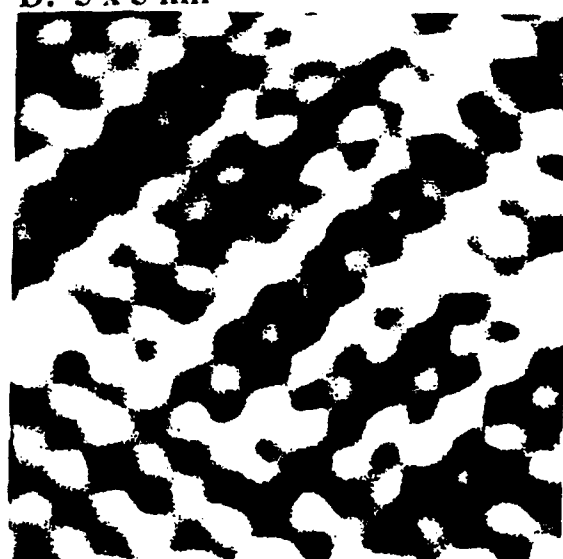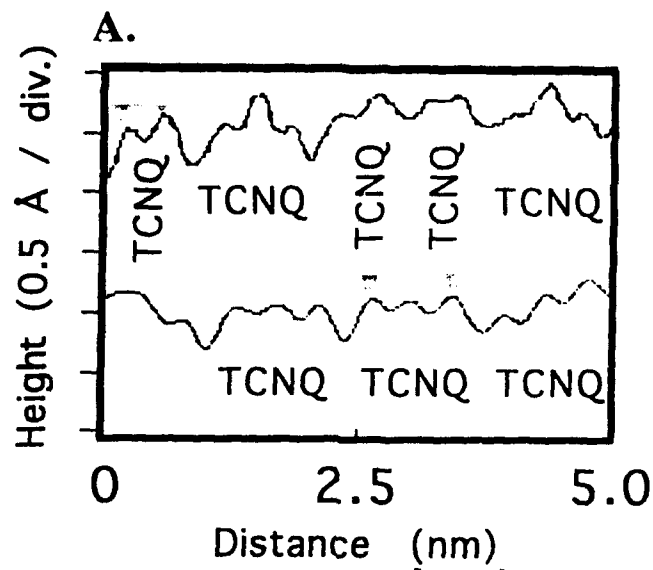
B. 4.5 x 4.5 nm²

C. 5 x 5 nm²
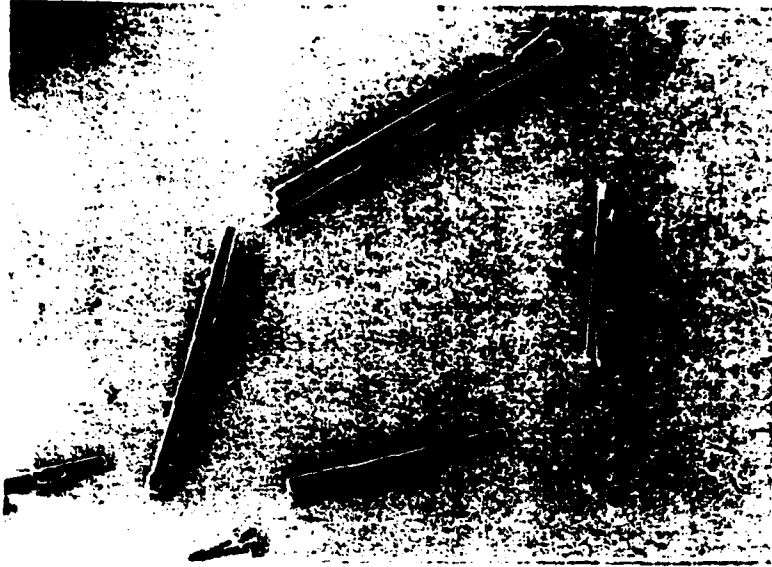

Hossick Schott. Ward Figure 6

Hossick Schott, Ward   Figure 7
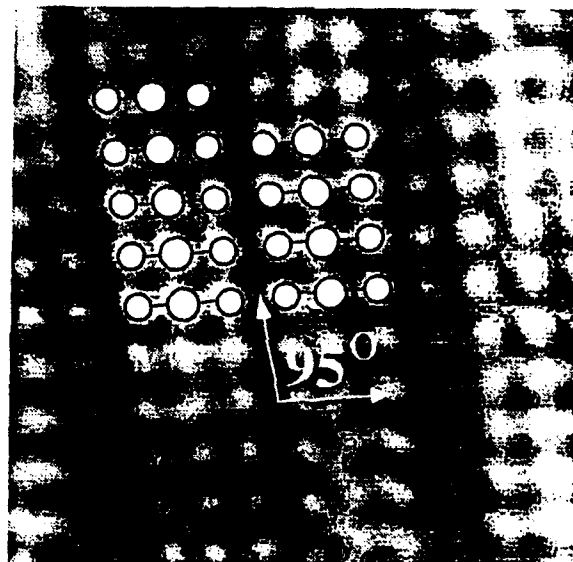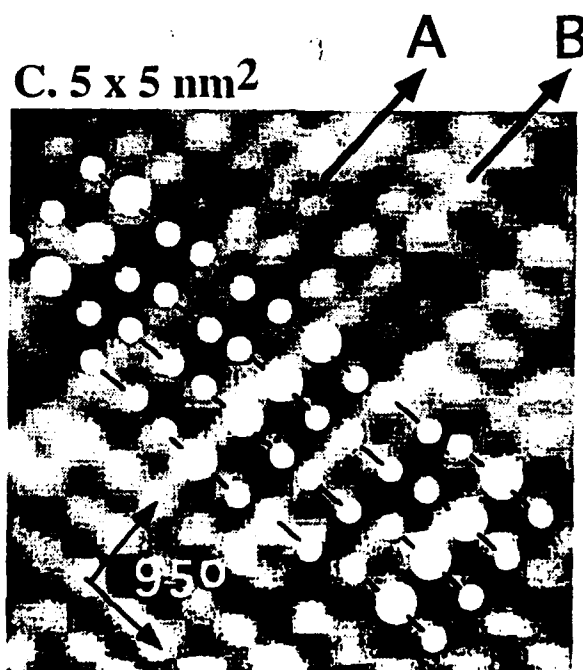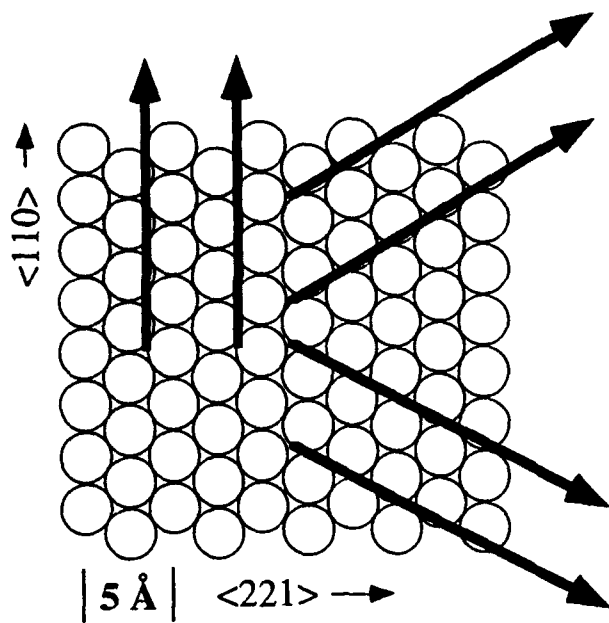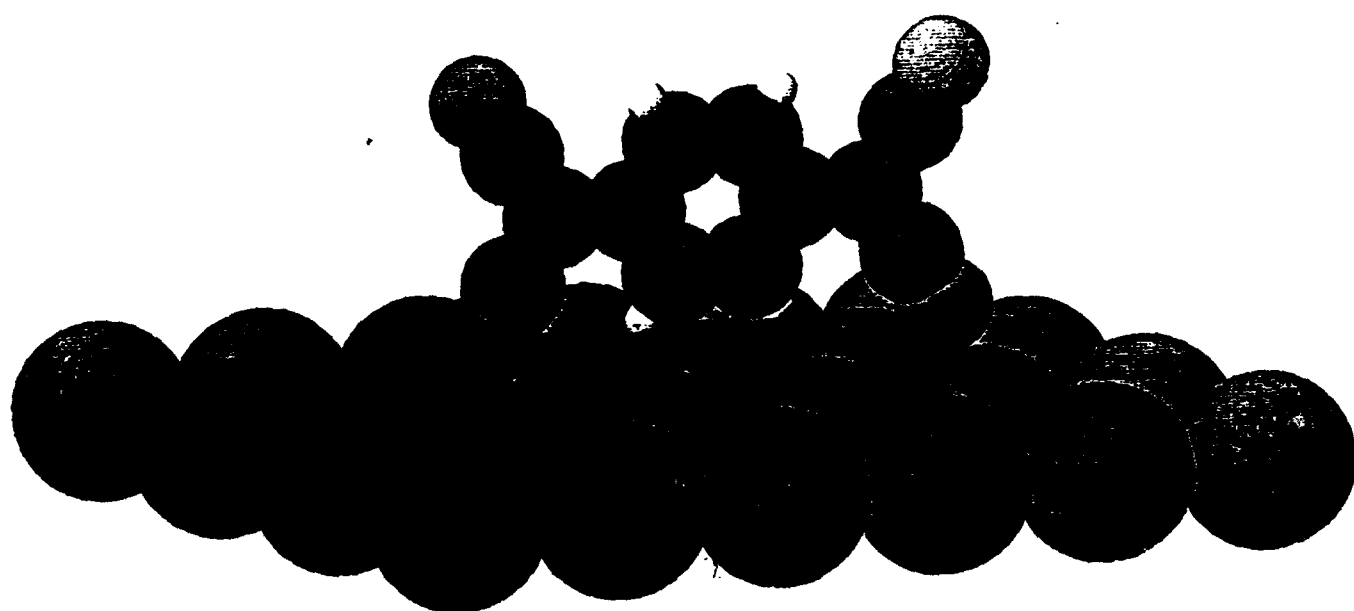
Hossick Schott, Ward   Figure 8

A. 100 x 107 μm

B. 60 x 41 μm²

Hossick Schott, Ward   Figure 9